MNRAS **000**, 1–11 (2017) Preprint 29 October 2017 Compiled using MNRAS LATEX style file v3.0

Overdensity of galaxies in the environment of quasar pairs

A. Sandrinelli[1,2]★, R. Falomo[3], A. Treves[1,2], R. Scarpa[4], M. Uslenghi[5]
[1]*Università degli Studi dell'Insubria, Via Valleggio 11, I-22100 Como, Italy*
[2]*INAF - Istituto Nazionale di Astrofisica, Osservatorio Astronomico di Brera, Via Emilio Bianchi 46, I-23807 Merate, Italy*
[3]*INAF - Istituto Nazionale di Astrofisica, Osservatorio Astronomico di Padova, Vicolo dell'Osservatorio 5, I-35122 Padova, Italy*
[4]*IAC - Instituto de Astrofisica de Canarias, C/O Via Lactea, s/n E38205 - La Laguna, Tenerife, España*
[5]*INAF-IASF - Istituto Nazionale di Astrofisica, Istituto di Astrofisica Spaziale e Fisica Cosmica, via E. Bassini 15, I-20133 Milano, Italy*

Accepted XXX. Received YYY; in original form ZZZ

ABSTRACT
We report on a study of the galaxy environments of low redshift physical quasars pairs. We selected 20 pairs having projected separation < 0.5 Mpc and difference of systemic velocity < 800 km s^{-1}. Using SDSS images we evaluated the galaxy overdensity around these quasars in pairs and then compare it with that of a sample of isolated quasars with same redshift and luminosity. It is found that on average there is a systematic larger overdensity of galaxies around quasars in pairs with respect to that of isolated quasars. This may represent a significant link between nuclear activity and galaxy environment. However, at odds with that, the closest quasar pairs seem to inhabit poorer environments. Implications of present results and perspectives for future work are briefly discussed.

Key words: galaxies: active– galaxies: clusters, general– galaxies: groups, general– quasars, general

1 INTRODUCTION

Quasars (QSOs) are luminous and short-lived active galactic nuclei (AGNs). They are associated to massive black holes (BHs) in the center of galaxies powered by gas accretion and they are revealed by their huge luminosity (Salpeter 1964; Zel'dovich 1964; Lynden-Bell 1969). To supply the enormous amount of gas from kilo-parsec galaxy scale to the center, different physical processes are invoked for luminous QSOs. The most accredited models are those that involve major mergers of similar-mass gas-rich galaxies (see e.g. Di Matteo, Springel, & Hernquist 2005; Hopkins et al. 2008; Kormendy & Ho 2013, and references therein). As an alternative, models based on radiative instabilities funneling in the inner several kpc metal-rich stellar-remnant recycled gas (e.g Ciotti, Ostriker, & Proga 2010) have been developed. Less violent mechanisms, like minor mergers (e.g. Hopkins et al. 2008), or secular processes unrelated with the merging phenomenon (e.g. Cisternas et al. 2011) as disk and bar instabilities (e.g. Shlosman, Frank, & Begelman 1989; Bournaud et al. 2011; Kocevski et al. 2012) or stochastic events, are also considered sufficient for fuelling less luminous AGNs (see e.g. Heckman & Best 2014, for a review).

Merger events are thought to depend on the global properties of the galaxy environment (e.g. Kauffmann & Haehnelt 2000; Di Matteo, Springel, & Hernquist 2005). In a number of cases galaxies hosting QSOs are observed in interacting systems or in apparent merger products (e.g. Canalizo & Stockton 2001; Green et al. 2011; Kunert-Bajraszewska & Janiuk 2011; Shields et al. 2012). Nevertheless, a significant enhancement of merger features in the QSO hosts with respect to those in inactive galaxies was not observed (e.g. Dunlop et al. 2003; Mechtley et al. 2016; Villforth et al. 2017). It was also expected that QSOs should preferably reside overly clustered regions especially at high redshift (e.g Djorgovski et al. 1999; Volonteri & Rees 2006), given that mergers should be more frequent in denser environments. However, not concordant evidences of richer environments around single QSOs in comparison to inactive galaxies were found, both at high (e.g. Morselli et al. 2014; Simpson et al. 2014) and intermediate-low redshifts (e.g. Serber et al. 2006; Padmanabhan et al. 2009; Shen et al. 2013; Zhang et al. 2013; Karhunen et al. 2014; Krolewski & Eisenstein 2015; Jiang et al. 2016). Evidences for a connection between environment, mergers and QSOs remain inconclusive.

Because of the short nuclear activity lifetime, only a small fraction of massive galaxies are shining as QSOs. In spite of this, a significant number of probable physical QSO pairs, i.e. QSO likely to be mutually gravitationally bound, belonging to the same cosmological structure, were discovered on sub-Mpc scale (e.g. Hennawi et al. 2006; Myers et al. 2008; Hennawi et al. 2010; Sandrinelli et al. 2014). The presence of an enhanced excess of these QSO pairs down to a scale of few tens kpc enforced the scenario of tidal interactions in gas-driven mergers leading to the mutual triggering of the nuclear phase in both QSOs (e.g. Djorgovski 1991; Kochanek, Falco, & Muñoz 1999; Mortlock, Webster, & Francis 1999; Myers et al. 2008; Foreman, Volonteri, & Dotti 2009). In such a case, a comparable small-scale enhanced environment is expected. The simultaneous presence of two close QSOs could also be explained as a statistically predictable consequence of group-scale environ-

★ E-mail: asandrinelli@yahoo.it

Table 1. Quasar pair sample and properties.

QP	QSO_A (J2000)	z_A	QSO_B (J2000)	z_B	$\Delta\theta$	$R_\perp$	$\Delta V_\parallel$	ref_A	ref_B	ref_{QP}
					[']	[kpc]	[km s^{-1}]			
(a)	(b)	(c)	(d)	(e)	(f)	(g)	(h)	(i)	(j)	(k)
1	SDSS J001103.18+005927.2	0.48646	SDSS J001103.48+010032.6	0.48636	65	394	20 ± 30	Sc10	P17	S14
2	SDSS J011757.99+002104.1	0.61127	SDSS J011758.83+002021.4	0.61286	45	300	300 ± 50	Sc10	Sc10	H06
3	SDSS J022610.98+003503.9	0.42396	SDSS J022612.41+003402.2	0.42383	66	363	25 ± 40	P17	Sc10	S14
4	SDSS J023328.44−054604.4	0.49445	SDSS J023331.05−054550.9	0.49394	41	249	100 ± 20	P17	P17	S17
5	SDSS J074759.02+431805.3	0.50117	SDSS J074759.65+431811.4	0.50175	8.9	56	115 ± 25	Sc10	Sc10	H06
6	SDSS J074843.02+361258.7	0.65399	SDSS J074843.12+361219.4	0.64959	39	273	795 ± 35	P17	Sc10	S17
7	SDSS J082439.83+235720.3	0.53526	SDSS J082440.61+235709.9	0.53676	16	94	290 ± 20	Sc10	Sc10	H06
8	SDSS J084541.18+071050.3	0.53755	SDSS J084541.52+071152.3	0.53516	62	393	470 ± 50	Sc10	Sc10	H06
9	SDSS J085625.63+511137.0	0.54240	SDSS J085626.71+511117.8	0.54316	23	139	150 ± 20	Sc10	Sc10	H06
10	SDSS J093847.45+462328.2	0.57707	SDSS J093853.83+462310.8	0.57734	68	448	50 ± 25	P17	P17	S17
11	SDSS J095137.00−004752.9	0.63395	SDSS J095139.39−004828.7	0.63691	50	346	540 ± 25	P17	P17	S14
12	2QZ J115240.09−003032.8	0.55375	SDSS J115240.52−003004.3	0.55209	29	188	320 ± 60	C04	Sc10	H06
13	SDSS J115822.77+123518.5	0.59572	SDSS J115822.98+123520.3	0.59690	3.6	24	220 ± 60	M08	M08	M08
14	SDSS J124031.42+111848.9	0.58480	SDSS J124032.67+111959.2	0.58404	73	479	145 ± 60	P17	P17	S17
15	SDSS J124856.55+471827.7	0.43859	SDSS J124903.33+471906.0	0.43861	79	447	5 ± 15	Sc10	Sc10	F11
16	SDSS J125454.86+084652.1	0.43977	SDSS J125455.09+084653.9	0.43969	3.8	22	430 ± 70	P17	Sc10	G10
17	2SLAQ J133350.41−003309.3	0.60697	2SLAQ J133351.17−003248.3	0.61030	24	160	620 ± 45	C09	C09	S17
18	SDSS J141855.41+244108.9	0.57305	SDSS J141855.53+244104.6	0.57511	4.5	29	390 ± 30	Sc10	M08	M07
19	SDSS J155330.22+223010.2	0.64127	SDSS J155330.55+223014.3	0.64223	5.9	42	175 ± 15	Sc10	P17	S14
20	SDSS J164311.34+315618.4	0.58653	SDSS J164311.38+315620.6	0.58636	2.3	15	30 ± 30	Sc10	B99	Mo99

(a) QSO pair (QP) identifier. (b) and (d) Names of QSOs from SDSS, 2QZ and 2SLAQ surveys. (c) and (e) Quasar redshifts derived from [OIII]λ5007 Å lines, see Sections 2 and 3.2. Intrinsic wavelength-calibration uncertainties are added in quadrature to the line position errors. (f) Angular separation between the two QSO pair components. (g) Proper traverse separation. (h) Radial velocity difference derived from data in columns (c) and (e). (i) and (j) References of the spectroscopic information used for the QSO pair search. (j) Reference of the first spectroscopical identification as a QSO pair.
References: B99: Brotherton et al. (1999); C04: Croom et al. (2004), 2dF QSO Redshift Survey (2QZ); C09: Croom et al. (2009), 2dF SDSS LRG (luminous red galaxy) and QSO (2SLAQ) survey; F11: Farina, Falomo, & Treves (2011); G10: Green et al. (2010); H06: Hennawi et al. (2006); Mo99: Mortlock, Webster, & Francis (1999); M07: Myers et al. (2007); M08: Myers et al. (2008); P17: Pâris et al. (2017), SDSS Quasar Catalog Data Release 12 (DR12Q); S14: Sandrinelli et al. (2014); Sc10: Schneider et al. (2010), SDSS Quasar Catalog Data Release 7 (DR7Q); S17: This work.

ments, in which small scale galaxy overdensities make mergers more likely to occur (e.g. Hopkins et al. 2008), or as a manifestation of the clustering properties of the dark matter halos hosting the QSOs (e.g. Di Matteo, Springel, & Hernquist 2005; Richardson et al. 2012). In the sketched pictures, QSO pairs constitute special cases to probe the quasar phenomenon. They could pose constraints on how, and to what extent, the galaxy environment is connected to the QSO activation, or clear up if quasar phase is stochastic process that every luminous galaxy in a typical galaxy cluster can experience. In the latter case, QSO pairs simply could derive from two galaxies simultaneously active for a period.

The QSO pairs environment has been investigated only in a few papers due to the lack of large samples and suitable data, resulting on average in a poor enhanced environment of galaxies at small scale, although signatures of galaxy clusters were detected in some cases. No enhancement in the galaxy density around a luminous z=4.25 QSO pair was found by Fukugita et al. (2004). Boris et al. (2007) explored the photometrical properties of four fields around QSO pairs at z$\lesssim$1 with separations of about 1 Mpc, leading to mixed results. In a study on six physical QSO pairs at z$\leqslant$0.8 drawn from the Sloan Digital Sky Survey (SDSS), Farina, Falomo, & Treves (2011) reported one case of pair in a significant overdense group of galaxies and dynamical evidences of mass exceeding that observed around other targets. Green et al. (2011), searching for signs of galaxy clusters associated to 7 close QSO pairs at z$\sim$1, did not detect such an evidence. Sandrinelli et al. (2014) investigated the environment of 14 physical SDSS QSO pairs at z$<$ 0.85 and found that they are harbored on average in regions of modest galaxy overdensity extending up to $\sim$0.5 Mpc, suggesting that the rare activation of two QSOs with small physical separation does not require an extraordinary environment. Recently, Onoue et al. (2017), applying less stringent constraints than ours (see Section 2) in defining QSO pairs, investigated the overdensities around associations of two QSOs extracted from the SDSS-III BOSS Survey in the DR12Q catalog (Pâris et al. 2017) with cluster-scale separation, as possible massive proto-clusters tracers. Focusing on the 33 pairs at $z \sim 1$, they reported evidence of enhanced environments in $\sim$ 20 % of cases. At higher z (3$<$z$<$4) they also detected two QSO pairs in a significant overdense environment. Rare cases of associations with more than two QSOs have been observed at $1.5 \lesssim z \lesssim 2$ by Djorgovski et al. (2007), Farina et al. (2013), and Hennawi et al. (2015) in very different environments (from poor to substantially overdense). In general, in previous works no exhaustive conclusion has been yielded on the subject.

To further investigate a possible link between the environment and the quasar activity, in this work we use SDSS images to analyze the environment properties at $\sim$ 1 Mpc-scale of a homogeneous sample of 20 reliable QSO physical pairs at $0.4 < z \lesssim 0.65$, selected from all the available QSO datasets (Section 2). The redshift range was chosen to better reveal possible environmental galaxy excess on the SDSS images. We complement SDSS imaging (Subsection 3.1) and spectroscopic studies with high quality optical spectroscopy gathered at Gran Telescopio CANARIAS (GTC) in La Palma (Subsection 3.2). As comparison sample, a purpose-built

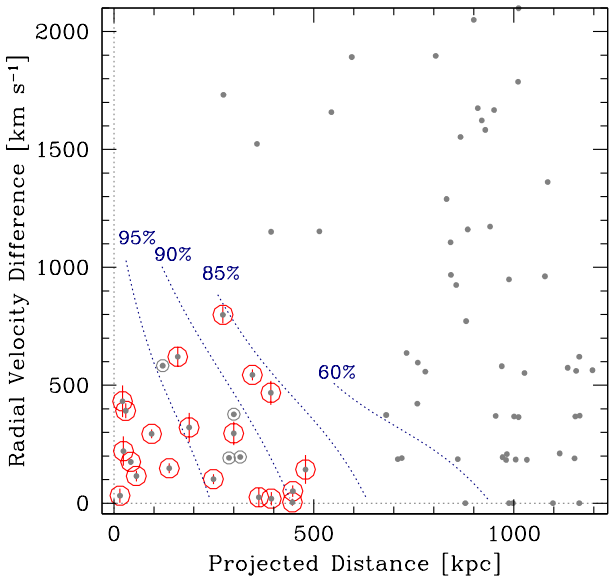

Figure 1. Distribution in the $R_\perp - \Delta V_\parallel$ plane of QSO pairs at 0.4 < z < 0.66 (grey dots). The percentage of the QSO pairs expected to be physical systems ranges between the reported values. The pairs investigated in this work are marked by red large circles. Excluded candidates (see text) are surrounded by grey small circles.

sample of 200 isolated QSOs drawn from SDSS archives, matching in redshift and luminosity with the QSO in pairs was selected (Section 4). For the QSO pairs we perform a detailed analysis of the clustering (Sections 5 and 6) of galaxies and compare the results with those derived from the control sample of isolated QSOs. The results and their implications are discussed (Section 7).

In this work we assume a concordant cosmology: $H_0 = 70$ km s^{-1} Mpc^{-1}, $\Omega_m = 0.30$ and $\Omega_\Lambda = 0.70$.

2 THE SAMPLE

We searched for physical QSO pair candidates following the procedure outlined in Sandrinelli et al. (2014). The starting dataset is based on the spectroscopic QSOs collected in The Million Quasars (MILLIQUAS) Catalog, Versions 3.9-4.3 (Flesch 2015), containing more than 420,000 QSOs from literature.

We expected to reach apparent magnitudes of $\sim$ 22 in the SDSS i-band images (see Section 5). At these magnitudes, we wished to detect environmental galaxies up to a limit $\gtrsim$ M* (M*=−21.70 mag, Montero-Dorta & Prada 2009) around the highest redshift QSO in our sample. We wanted also to limit the number of detectable background galaxies, which could overshadow possible local overdensity effects at low redshifts. With these aims, we restricted the QSO pair sample search to $\sim$ 21,500 QSOs at 0.4 < z $\lesssim$ 0.65. In addition, at these redshifts QSOs show the [OIII]λ5007 line well inside the optical spectral range, allowing us to improve the accuracy in measuring their systemic radial velocity for a more reliable selection of probable bound QSO pairs (see below, and also see Section 3.2).

For each association of two QSOs, constructed by coupling each QSO with all the others, we evaluate projected separations $R_\perp$ and differences of radial velocities $\Delta V_\parallel$ between the two components. To assemble a population of binary QSOs likely to be gravitationally bound, in each bi-dimensional bin of the $R_\perp$-$\Delta V_\parallel$ plane (Figure 1) the excess of observed QSO pairs with respect those obtained randomly permuting the redshifts (e.g. Zhdanov & Surdej 2001) is estimated. This allows us to trace the loci in $R_\perp$-$\Delta V_\parallel$ plane where the probability for a QSO pair of being not a chance superposition is higher than a fixed constant value ξ. For our search we choose ξ>85%.

After a first selection based on redshifts in literature, 24 QSO physical pairs candidates were found. Four of them were discharged for dubious classification of one component after visual inspection of the spectra drawn from SDSS[1]. A dedicated complementary spectroscopical program was undertaken at the Gran Telescopio Canarias (GTC, Subsection 3.2) for a number of the remaining pairs, not investigated in Sandrinelli et al. (2014). We re-evaluate the positions of all the selected QSO pairs in the $R_\perp$-$\Delta V_\parallel$ plane, by measuring $\Delta V_\parallel$ from the narrow forbidden[OIII]λ5007 emission line, which arises from regions where gas is predominantly orbiting in the host galaxy potential and therefore is a good z estimator (e.g. Hewett & Wild 2010; Liu et al. 2014). The wavelength of the line was measured with the procedure described in Farina, Falomo, & Treves (2011).

All 20 pairs (z_{ave}=0.55) were confirmed in the final sample of physical QSO pairs candidates (see Section 3.2), of which 5 are new, not discussed before. The sample is given in Figure 1 and Table 1, where $\Delta V_\parallel$ from [O III]λ5007 measurements are reported. It contains 9 pairs already studied in Sandrinelli et al. (2014). Seven pairs have $R_\perp$ < 100 kpc. The sample is largely radio-quite dominated[2], with only one QSO detected as radio-loud (J164311.34+315618.4, see also Appendix A).

3 OBSERVATIONS

3.1 SDSS Imaging

Calibrated, sky-subtracted i-band images of the QSO fields were retrieved from SDSS archives. At the average redshift of the QSO data set, this corresponds to observe in the SDSS g filter at rest frame. Images have an exposure time of 54 s and a mean seeing of 1.04 arcsec. We drew photometrical information from SDSS DR12 catalogues, where objects classifications are based on the difference between the cmodelMag (composite de Vaucouleurs and exponential model) and the Point Spread Function (psf) magnitudes. We obtained position and i-band photometry of QSOs and of all primary objects photometrically classified as galaxies (`type = 3`) in the fields. The photometrical properties of the QSO pair sample given in Table 2 complement those already reported in Sandrinelli et al. (2014). Apparent magnitudes (psfmag) are taken from SDSS database. Absolute magnitudes M_i are extinction corrected on the basis of SDSS values following Schlegel, Finkbeiner, &

[1] The discarded QSO physical pair candidates are J015628.41+174957.6 (SDSS DR10, Ahn et al. 2014), J091442.32+000637.1 (SDSS DR3, Abazajian et al. 2009), J103834.84+595725.7 and J121336.12+463355.8 (SDSS DR12, Alam et al. 2015). Their spectra are characterized by flat-shape continuum, absence of broad lines and suppressed MgII emission line. We note that none of these objects is recovered in SDSS DR7Q (Schneider et al. 2010) and DR12Q (Pâris et al. 2017).

[2] Data from VLA FIRST Survey (`http://sundog.stsci.edu`) and NRAO VLA Sky Survey (`http://www.cv.nrao.edu/nvss`) catalogues.

Table 2. Photometrical properties of the subsample of newly investigated QSO pairs.

QP	i_A	$M_A(i)$	i_B	$M_B(i)$	$m_{i,50\%}$	$M_{i,50\%}$
	[mag]	[mag]	[mag]	[mag]	[mag]	[mag]
(a)	(b)	(c)	(d)	(e)	(f)	(g)
2	19.99	−22.87	18.25	−24.62	22.2	−20.68
4	20.31	−21.97	18.45	−23.83	22.0	−20.33
6	19.97	−23.14	20.19	−22.91	22.0	−21.09
10	19.30	−23.35	19.97	−22.70	21.9	−20.83
12	20.04	−22.53	18.84	−23.72	22.1	−20.52
13	19.49	−23.30	19.77	−23.00	21.8	−21.03
14	19.99	−22.76	20.18	−22.55	21.9	−20.87
16	19.29	−22.69	17.06	−24.91	21.9	−20.14
17	19.96	−22.90	20.39	−22.47	21.9	−20.97
18	18.94	−23.72	19.89	−22.77	22.0	−20.72
20	18.80	−23.95	19.51	−23.23	22.1	−20.68

(a) QSO pair identifier. (b) and (d) SDSS i-band apparent magnitude (psfmag) of QSO A and B, respectively; (c) and (e) Extinction and k-corrected absolute magnitude of QSO A and B, respectively. (f) and (g) Apparent SDSS magnitude threshold and correspondent absolute magnitude, see Section 5.

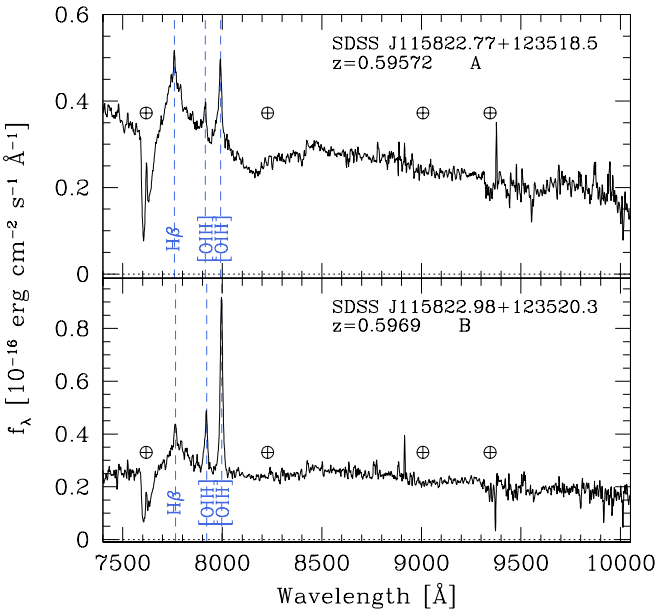

Figure 2. GTC spectra of the QSO pair QP13 (see also Appendix A). The two components have a projected separation of 3.6″, corresponding to 24 kpc at the redshift of the pair, and a difference of radial velocity of (220 ± 60) km s^{-1}(Table 1). The most prominent emission features are marked. The main telluric bands are indicated by ⊕. The comparison between the two spectra allows us to exclude that the QSO pair is a gravitationally lensed image.

Davis (1998). *K*-corrections are also applied by adopting the template spectra of Francis et al. (2001) and Mannucci et al. (2001) for QSOs and galaxies, respectively, and the i-band filter response. The mean i-band absolute dereddened magnitude for the full sample is $M_{ave}(i) = -23.16 \pm 0.12$ mag, where the uncertainty is the standard error of the mean.

3.2 Optical spectroscopy

Among the selected QSO pairs in Table 1, five lack of spectra in SDSS archives for at least one QSO member (see Table 3). Three of them have small component separations ($2'' < \Delta\theta < 10''$) and they are of special interest. Although in general considered as highly probable close binaries rather than lensed sources (see Table 1 and Appendix A for more details), the lensing hypothesis was not excluded for some cases (QSO pairs QP13 and QP18, Myers et al. 2008, 2007), deserving higher resolution spectroscopy. Another QSO pair is newly discovered (QP17). Both its QSOs were independently observed in the 2SLAQ Survey (Croom et al. 2009). For the remaining pairs (QP2, QP14, QP16, of which the last one is another close pair), we were interested in obtaining reliable measures of the [OIII]λ5007 region.

For these QSO pairs we secured optical spectra at the 10.4m GTC, located in Roque de los Muchachos, La Palma, using the OSIRIS spectrograph (Cepa et al. 2003). Intermediate resolution (R ∼2200) observations were performed using R2500I or R2500R grisms in order to detect the [OIII]λ5007 Å line region. For each QSO pair the slit was oriented to simultaneously secure the spectra of both objects, and three individual spectra were obtained. We reduced data by using the standard IRAF recipes and applied flux corrections using SDSS photometry. Journal of GTC observation is given in Table 3. In Figure 2 we show as example the GTC spectra of the QSO pairs QP13. The other ones are illustrated in Figure A1 in Appendix A, where notes on some individual paired targets are also reported. Detailed comparisons between the two GTC optical spectra of each pair allow us to confirm that all our targets are physical QSO pair candidates. In particular, the QSOs with small angular separation, are paired QSOs rather than lensed images, see Appendix A.

4 A COMPARISON SAMPLE OF ISOLATED QUASARS

We aim to probe whether the clustering of galaxies in ∼1 Mpc-scales region hosting QSOs is sensitive to the presence of QSO pairs. In particular, we compare the average overdensity distribution of galaxies around individual QSOs in pairs with that of 200 isolated QSOs, which are well matched with the paired QSOs in terms of redshift and luminosity. The sample was assembled from SDSS DR12 Catalog[3] of spectroscopical confirmed QSOs, following Subsection 3.1 for photometrical measurements. We randomly extracted ten isolated sources for each QSO pair, drawing five objects among those at distances $\Delta z < 0.02$ and $\Delta M_i < 0.35$ mag from each QSO in pairs in the redshift-luminosity plane (see Figure 3). Before to confirm objects in the sample, optical SDSS spectra were visually checked to secure identification, to reliably estimate the emission redshift, and to identify peculiar features. The two samples of paired and isolated QSOs also well match in terms of distributions of host galaxy luminosity, both ranging from −21 mag to −25.5 mag around the mean value $<M(r)_{host}>\sim -23.3$ mag. Details on the nuclear/host luminosity decomposition of the QSO images are given in Appendix B.

[3] `http://www.sdss.org/dr12/algorithms/boss-dr12-quasar-catalog`

Table 3. Journal of GTC observations.

QP	Date	Seeing [″]	Slit [″]	t_{exp} [s]	Grism	$SNR_{(A)}$	$SNR_{(B)}$	SDSS
(a)	(b)	(c)	(d)	(e)	(f)	(g)	(h)	(i)
2	2015 Dec 28	1.5	1.0	900	R2500I	12	25	A, B
12	2016 Mar 19	0.9	1.0	980	R2500I	10	16	B
13	2015 Apr 10	1.4	1.2	800	R2500I	20	14	
14	2015 May 10	1.0	1.2	900	R2500I	14	10	A, B
16	2016 Feb 06	1.3	1.0	900	R2500R	31	70	A, B
17	2016 Mar 26	1.0	1.0	900	R2500I	10	8	
18	2015 May 10	0.9	1.2	1000	R2500I	25	10	A
20	2015 Apr 10	1.3	1.2	500	R2500I	26	15	A

(a) QSO pair identifier. (b) Date of observations; (c) Mean seeing during the observations; (d) Slit width; (e) Exposure time; (f) Grism; (g) and (h) Average signal-to-noise ratio of the spectrum of QSO A and QSO B, respectively; (i) QSO spectroscopically observed by SDSS.

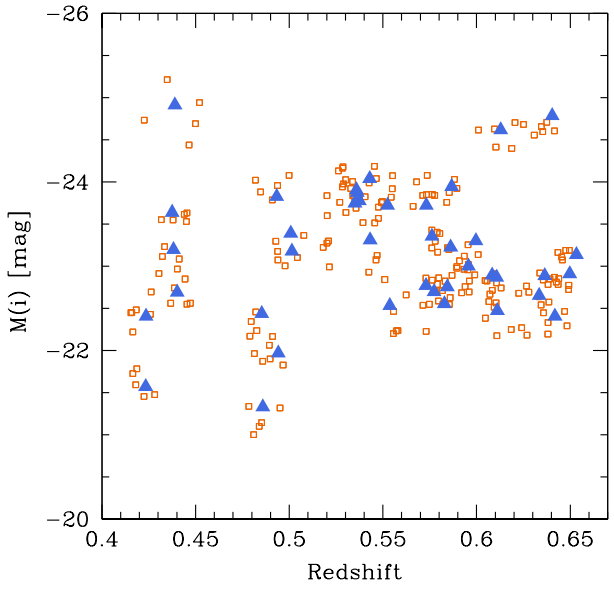

Figure 3. The QSO samples in the M(i)-redshift plane. Blue triangles are the QSOs in pairs. The 200 isolated QSOs of the comparison sample, matched in redshift and luminosity with QSOs in pairs, are reported as orange open squares.

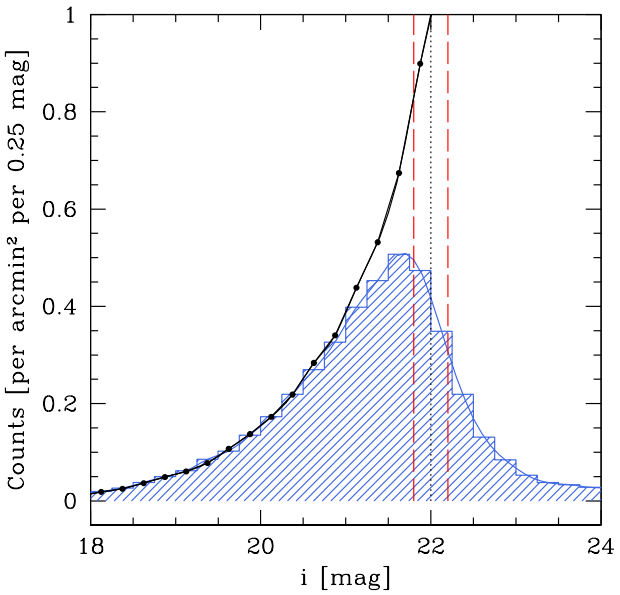

Figure 4. Mean i-band magnitude distribution of the galaxies in the background regions around the QSO pairs (see text). Black solid line represents the expected distributions of galaxies (Capak et al. 2007). Dotted line marks the 50% completeness limit $m_{i,50\%}$, see Table 2. Red large-dashed lines indicate the minimum and the maximum magnitude thresholds in the sample.

5 GALAXY ENVIRONMENT OF THE QUASAR PAIRS

In order to characterize the environment around QSOs in pairs and around isolated QSOs, we estimated the surface density of galaxies with respect the distance from the targets using the SDSS objects classified as galaxies, see Section 3.1. The midpoint of each pair was used to evaluate the background galaxy density at angular distances between 7 and 15 arcmin, corresponding to a projected distance between ∼ 2.5 and ∼ 5 Mpc for the nearest pair. The environment around QSOs is then evaluated around the position of each individual QSO.

To take into account the completeness of the SDSS galaxy catalogues, galaxy surface densities are estimated by counting galaxies brighter than a magnitude limit. This is fixed for each field at the magnitude $m_{i,50\%}$, where the differential magnitude distribution of the observed galaxies in the background region drops to 50% of that estimated by the deep galaxy survey in Capak et al. (2007)[4]. In our SDSS i-band images the threshold magnitudes are distributed around the mean value $mi_{50\%,ave}$ = 22.0 ± 0.02 mag (see Table 2). At these thresholds we can observe galaxies brighter than ∼M*+2

[4] Durham University Cosmology Group, references and data in `http://astro.dur.ac.uk/~nm/pubhtml/counts/counts.html`

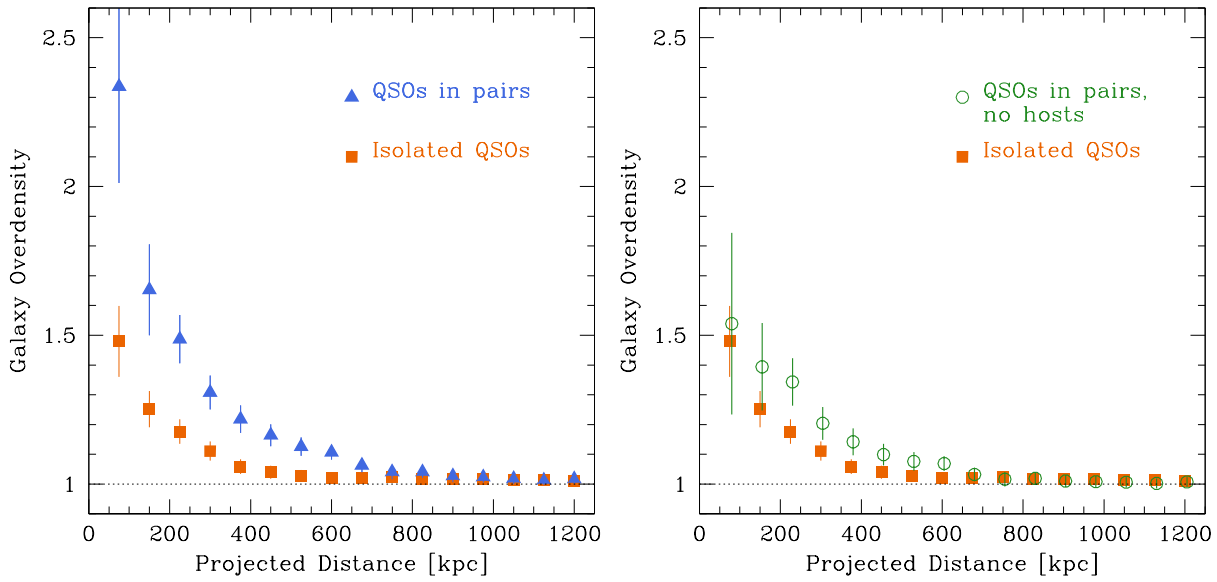

Figure 5. Mean cumulative galaxy overdensities around QSOs in pairs as a function of the projected distance from the QSO. The cases of inclusion or exclusion of the host galaxy of the companion QSO is reported respectively in the *left panel* (blue triangles), and in the *right panel* (green circles). Mean cumulative galaxy overdensity around 200 isolated QSOs of the comparison sample, matching with the QSO pairs in luminosities and redshifts, is also plotted (orange squares). The uncertainties are the standard errors of the mean evaluated in each bin.

Table 4. Statistics of galaxies in the QSO pair environments.

QP	n_{bg} [arcmin^{-2}]	n_{bg} [Mpc^{-2}]	$N_{0.25}$ A	$N_{0.25}$ B	N_I	$N_{bg,I}$	$\mathcal{N}_{0.25}$ A	$\mathcal{N}_{0.25}$ B	$G_{0.25}$ A	$G_{0.25}$ B	$G_{0.5}$ A	$G_{0.5}$ B
(a)	(b)	(c)	(d)	(e)	(f)	(g)	(h)	(i)	(j)	(k)	(l)	(m)
1	3.6 ± 0.1	27.4 ± 0.8	7	6	0	0.6	7.0	6.0	1.30 ± 0.04	1.11 ± 0.02	1.21 ± 0.03	0.70 ± 0.02
2	3.9 ± 0.3	23.7 ± 1.7	8	7	3	1.3	7.2	6.2	1.54 ± 0.13	1.32 ± 0.08	1.17 ± 0.09	1.01 ± 0.08
3	4.0 ± 0.3	36.2 ± 2.3	9	12	3	1.2	8.1	11.1	1.14 ± 0.08	1.56 ± 0.09	1.17 ± 0.08	1.31 ± 0.09
4	3.7 ± 0.2	27.9 ± 1.2	9	9	3	2.2	8.6	8.6	1.57 ± 0.06	1.57 ± 0.05	1.17 ± 0.05	1.12 ± 0.05
5	3.2 ± 0.2	24.0 ± 1.3	8	9	7	4.0	6.5	7.5	1.38 ± 0.08	1.59 ± 0.06	1.07 ± 0.06	1.07 ± 0.06
6	3.3 ± 0.2	19.3 ± 1.1	9	5	2	1.3	8.7	4.7	2.28 ± 0.13	1.23 ± 0.09	1.12 ± 0.07	1.52 ± 0.09
7	3.6 ± 0.3	24.9 ± 1.7	11	7	6	3.7	9.9	5.9	2.02 ± 0.14	1.20 ± 0.10	1.34 ± 0.10	1.34 ± 0.10
8	3.5 ± 0.2	24.4 ± 1.2	5	7	1	0.5	4.8	6.8	0.99 ± 0.05	1.41 ± 0.05	0.88 ± 0.05	0.93 ± 0.05
9	3.3 ± 0.1	22.9 ± 0.9	4	4	2	2.9	4.0	4.0	0.89 ± 0.03	0.89 ± 0.03	0.84 ± 0.03	0.95 ± 0.03
10	3.3 ± 0.1	21.5 ± 0.7	7	4	1	0.2	6.6	3.6	1.56 ± 0.05	0.85 ± 0.03	1.41 ± 0.04	0.88 ± 0.03
11	3.1 ± 0.2	18.2 ± 0.9	7	4	2	0.7	6.3	3.3	1.78 ± 0.09	0.94 ± 0.07	1.20 ± 0.06	1.34 ± 0.07
12	4.3 ± 0.2	29.0 ± 1.2	14	16	8	3.0	11.5	13.5	2.02 ± 0.10	2.38 ± 0.07	1.30 ± 0.06	1.44 ± 0.07
13	2.9 ± 0.2	17.9 ± 1.4	8	6	4	3.3	7.7	5.7	2.18 ± 0.15	1.61 ± 0.13	1.52 ± 0.14	1.37 ± 0.13
14	3.2 ± 0.3	20.7 ± 1.7	4	7	0	0.05	4.0	7.0	0.98 ± 0.08	1.72 ± 0.08	1.17 ± 0.09	1.04 ± 0.08
15	3.9 ± 0.1	33.4 ± 0.9	9	9	1	0.3	8.6	8.6	1.32 ± 0.04	1.32 ± 0.03	1.20 ± 0.03	1.12 ± 0.03
16	3.2 ± 0.2	27.8 ± 1.9	8	7	6	5.2	7.6	6.6	1.39 ± 0.09	1.21 ± 0.06	0.96 ± 0.06	0.96 ± 0.06
17	2.9 ± 0.1	17.6 ± 0.6	8	4	2	2.1	8.0	4.0	2.32 ± 0.06	1.16 ± 0.04	1.09 ± 0.03	1.31 ± 0.04
18	3.3 ± 0.1	21.4 ± 0.6	2	2	1	3.9	2.0	2.0	0.48 ± 0.01	0.48 ± 0.03	1.01 ± 0.03	0.89 ± 0.03
19	3.1 ± 0.2	17.9 ± 1.2	11	11	9	3.1	8.1	8.1	2.29 ± 0.18	2.29 ± 0.11	1.43 ± 0.11	1.36 ± 0.11
20	3.4 ± 0.1	21.9 ± 0.7	7	7	6	4.1	6.1	6.1	1.41 ± 0.04	1.41 ± 0.02	0.87 ± 0.02	0.87 ± 0.02

Notes: The target host galaxy is excluded from the counts and companion host is included. Errors are calculated taking into account only the average background surface density uncertainties. (a) QSO pair identifier. (b) and (c) Surface density of galaxies in the background with i < $m_{i,50\%}$ in arcmin^{-2} and Mpc^{-2}, respectively. (d) and (e) Number of galaxies within 250 kpc from the QSO A and B, respectively. (f) Number of galaxies in the overlapping region. (g) Number of expected background galaxies in the overlapping region, see text. (h) and (i) Number of galaxies within 250 kpc from each QSO after subdivision of the excess of galaxies in common. (j) and (k) Galaxy overdensity within 250 kpc from the QSO A and B, corrected for the superposition of the companion environment. (l) and (m) The same as in columns (j) and (k) within 500 kpc.

at z=0.4, ~M*+1 at z=0.5 and ~M* at z=0.65. The mean distribution of galaxy magnitudes obtained from the background regions of the QSO pair sample is shown in Figure 4. We estimate the background surface density n_{bg} of galaxies by computing the median of the galaxy surface density observed in 1 arcmin-width annuli in the background area. The local cumulative[5] surface density $n(r)$ around each QSO is evaluated inside circular apertures of radius r, with r ranging by steps of 75 kpc and covering the inner 2.5 Mpc.

[5] Since each aperture includes the inner ones, we refer to quantities derived from this approach as *cumulative*, see Karhunen et al. (2014).

The target QSO host galaxy is excluded. The cumulative overdensity profile of galaxies is then defined as $n(r)/n_{bg}$. In the case of QSO pairs, to take into account the contribution of the two sources, for each radius $n(r)$ is corrected by subdividing in equal number to each QSOs the excess of galaxies (over the background) in the region where the apertures overlap (see Sandrinelli et al. 2014). Hereafter, we refer to the overdensity as $G(r)$. For the case of QSOs in pairs, details of counts of individual QSOs contribution to the pair environment are reported in Table 4 for radius apertures of 250 kpc, and results are also given in the case of 500 kpc radius.

Because of the low statistics, the $G(r)$ distributions for each source appear rather noisy and significant differences among the various QSO are apparent. Therefore we have concentrated on the averaged cumulative profile evaluated of the entire sample of the 40 QSO belonging to pairs.

Our main result is that the galaxy overdensity of QSOs in pairs is clearly larger when compared with that derived from the comparison sample of isolated QSOs, as shown in Figure 5. We find that the mean galaxy overdensity around QSO in pairs within 0.25 Mpc is $<G_{0.25}>$ = 1.45±0.07 ($<G_{0.25}>$ = 1.33±0.08 if the companion host galaxy is excluded), while for the comparison sample we obtain $<G_{0.25}>$ = 1.13±0.04. The increase of overdensity in the case of paired QSOs at r=250 kpc is ∼ 25 %.

At ten kpc scales QSOs appear more clustered (e.g. Hennawi et al. 2006; Myers et al. 2007, 2008; Kayo & Oguri 2012; Eftekharzadeh et al. 2017) compared to the power-law extrapolation of clustering measurement at larger scales (Mpc, e.g. Porciani, Magliocchetti, & Norberg 2004). This may be interpreted as an indication of dissipative interactions (Djorgovski 1991; Kochanek, Falco, & Muñoz 1999; Myers et al. 2007) in a comparable-scale richer environment. Intriguingly, the immediate galaxy environment of the very close pairs in our sample ($R_\perp$ < 30 kpc) appears depleted. No galaxy is detected in the SDSS images up to projected distances $\lesssim$ 80 kpc. If we exclude the companion QSOs (to limit their influence on the cumulative numbering of the surrounding poor environment), the cumulative galaxy overdensity profile reveals a underdensity (G=0.5-1) with respect the background extending up to ∼100-150 kpc, followed by flat trend where $G(r) \sim 1$. If we focus on the entire environment surrounding both QSOs by measuring the overdensity from the midpoint of the pair, we find that it appears on average still underdense compared both to that of the remaining pairs and that of isolated QSOs up to distances of ∼ 300 kpc. However, it is worth noting that this result represents only an indication, since it is based on a very small number of QSOs.

6 NEAREST NEIGHBOR GALAXY ANALYSIS

We examine the SDSS photometrically classified galaxies in the immediate vicinity of our sampled QSOs searching for possible links between their properties and the QSO activity. In Figure 6 we compare the distributions of the projected distance of the 1st-nearest neighbor galaxy of paired QSOs with that of isolated ones. When the companion-QSO host galaxies are taken into account the 1st-nearest neighbor galaxies are found globally closer to paired QSOs (mean projected distance 61.0 kpc), with respect to isolated ones (mean 88.4 kpc), whose distribution extend for nearly twice the distance. About two thirds of 1st-nearest-neighbors of the QSOs in pairs (24 out of 40) are located at distances < 60 kpc, where strong interactions may be expected. Nearly half of them (11 out of 40) are the companion-QSO hosts in the closest pairs. The other ones, ∼ 33% of the total sample, are inactive galaxies, mainly con-

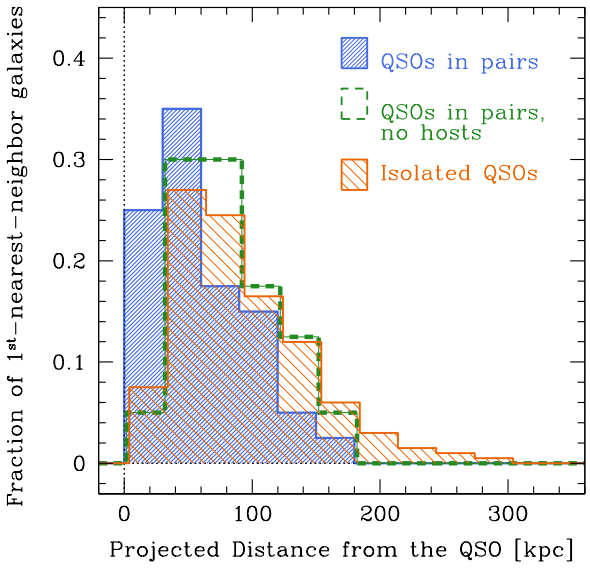

Figure 6. Normalized distributions of the projected distances from the QSOs of 1st-nearest-neighbor galaxies brighter than the magnitude threshold $m_{i,50\%}$, observed in the SDSS i-band images. Filled (blue) and dashed-contour (green) histograms refer, respectively, to the case of inclusion or exclusion of the host galaxy of the companion QSO from the 1st-nearest-neighbor search. The distribution around isolated QSOs is reported as the line-filled (orange) histogram.

centrated around 50 kpc from the QSO. This same fraction (69 out of 200) of closest companion galaxies is detected around single QSOs at these distances. The luminosity distributions of the 1st-nearest neighbors within 60 kpc range from −20 to −26 mag for both the samples, with differences toward higher luminosities in the case of paired QSOs, depending only on the host galaxy contribution.

In conclusion, the exclusion of the hosts from the search of the 1st-nearest neighbors makes the distance and luminosity distributions around QSOs in pairs indistinguishable from those around isolated QSOs.

7 DISCUSSION

We selected 20 low redshift ($z_{ave} \sim 0.5$) likely physical QSO pairs, with the aim of characterize the galaxy environment around each QSO and investigate if there is a connection between the environment properties and the QSO activity. These properties are compared to those of a consistent sample of isolated QSOs at the same redshifts and with similar global and host galaxy luminosities. Our results indicate that the galaxy environment of low redshift QSOs that are in pairs is, on average, richer than that around isolated QSOs (Figure 5). Moreover, based on the present data, there is a suggestion that the scenario could be more complex, depending on the pair separation. The comparison of our current results with previous studies on the QSO pair galaxy environment (Fukugita et al. 2004; Boris et al. 2007; Green et al. 2011; Farina, Falomo, & Treves 2011; Sandrinelli et al. 2014; Onoue et al. 2017) does not help to improve the understanding of the picture because of the relevant differences among these works (e.g. differences of redshift, QSO

luminosity, pair-member separation, difference of radial velocity, deepness of observation, etc..)

A local and overdense environment of galaxies could have a role on the generation of powerful QSO nuclear activity. The link between the richness of galaxy groups and the presence of an active nucleus could arise just by the higher probability of interaction in richer environments. However, it does not imply that in rich clusters of galaxies one expects to find many QSOs (e.g. Coldwell & Lambas 2006; Kauffmann et al. 2004). The most likely environments for interactions are poor groups (e.g. Silverman et al. 2009), in which galaxies have low relative velocities (e.g. Ostriker 1980; Kauffmann et al. 2004; Popesso & Biviano 2006) and more cold gas content (e.g. McNamara & Nulsen 2007). This is also consistent with models on the cosmological role of QSOs (e.g. Hopkins et al. 2008), where major mergers between gas-rich galaxies are expected to preferentially occur in small scale clustering excess. Our findings, although based on a small sample at low redshift, appear in agreement with the role of major merger in small group of galaxies for sustaining QSO activity (e.g. Hopkins et al. 2008).

We note that in the cases of closest QSO pairs (projected separations <30 kpc) the detection of a less dense environment is consistent with the fact that around these QSOs there is no evidence of extended X-rays emission (Green et al. 2011). The interpretation of the poor environment around very close QSO pairs is not trivial, since the probability of interactions should be enhanced by clustering excess on small scales. We may argue that these cases represent a situation where the nuclear activity is triggered by the mutual/contemporaneous interaction of two massive galaxies, or possibly also with other group-companion galaxies (see the case of QSO pair QP18 in Appendix A). If proved, the tendency of these rare QSO pairs to live in particularly modest environments may be supported by some kind of suppression effects, similar to those invoked in the models of e.g. Bonoli et al. (2009) and Fanidakis et al. (2013), where the QSO activities in haloes more massive then $\sim 10^{12}$-10^{13} $M_{\odot}$ are inhibited due to the suppression of gas cooling by active galactic nucleus feedback.

As the general indication is that pairs inhabit small groups of galaxies extending up to few hundreds kpc rather than clusters, at least in the redshift range of our investigation, they cannot be used for locating large-scale structures, as suggested by Djorgovski et al. (1999) for the case of high redshift QSOs, even if more than one QSO may co-exists in massive structure (e.g. Onoue et al. 2017).

Our results and interpretations could be probed using a larger sample of QSO pairs, extending also at larger z, and an adequate comparison of a suitable sample of isolate QSOs. A better characterization of the environment is now feasible with large telescopes equipped with Multi-Object Spectroscopy at optical and near-IR wavelengths. Physical evidences of whether and which galaxies are associated with QSOs, their velocity dispersion and dynamical mass compared with the expectation from models may be achieved. The concurrent search for environmental galaxy signatures of recent star formation through the Hα emission line will allow us to fully explore/study the environment-activity relations.

ACKNOWLEDGEMENTS

We thank the anonymous referee for useful comments and suggestions which enabled us to improve the paper.

Quasars in our QSO pair sample were published as the Half Million Quasars catalog (versions 3.9-4.3 Flesch 2015).

Funding for the Sloan Digital Sky Survey IV has been provided by the Alfred P. Sloan Foundation, the U.S. Department of Energy Office of Science, and the Participating Institutions. SDSS acknowledges support and resources from the Center for High-Performance Computing at the University of Utah. The SDSS web site is www.sdss.org. SDSS is managed by the Astrophysical Research Consortium for the Participating Institutions of the SDSS Collaboration including the Brazilian Participation Group, the Carnegie Institution for Science, Carnegie Mellon University, the Chilean Participation Group, the French Participation Group, Harvard-Smithsonian Center for Astrophysics, Instituto de AstrofŠsica de Canarias, The Johns Hopkins University, Kavli Institute for the Physics and Mathematics of the Universe (IPMU) / University of Tokyo, Lawrence Berkeley National Laboratory, Leibniz Institut f§r Astrophysik Potsdam (AIP), Max-Planck-Institut f§r Astronomie (MPIA Heidelberg), Max-Planck-Institut f§r Astrophysik (MPA Garching), Max-Planck-Institut f§r Extraterrestrische Physik (MPE), National Astronomical Observatories of China, New Mexico State University, New York University, University of Notre Dame, ObservatŮrio Nacional / MCTI, The Ohio State University, Pennsylvania State University, Shanghai Astronomical Observatory, United Kingdom Participation Group, Universidad Nacional AutŮnoma de MŐxico, University of Arizona, University of Colorado Boulder, University of Oxford, University of Portsmouth, University of Utah, University of Virginia, University of Washington, University of Wisconsin, Vanderbilt University, and Yale University.

REFERENCES

Abazajian K. N., et al., 2009, ApJS, 182, 543-558
Ahn C. P., et al., 2014, ApJS, 211, 17
Alam S., et al., 2015, ApJS, 219, 12
Bonoli S., Marulli F., Springel V., White S. D. M., Branchini E., Moscardini L., 2009, MNRAS, 396, 423
Boris N. V., Sodré L., Jr., Cypriano E. S., Santos W. A., de Oliveira C. M., West M., 2007, ApJ, 666, 747
Bournaud F., Dekel A., Teyssier R., Cacciato M., Daddi E., Juneau S., Shankar F., 2011, ApJ, 741, L33
Brotherton M. S., Gregg M. D., Becker R. H., Laurent-Muehleisen S. A., White R. L., Stanford S. A., 1999, ApJ, 514, L61
Canalizo G., Stockton A., 2001, ApJ, 555, 719
Capak P., et al., 2007, ApJS, 172, 99
Cepa J., et al., 2003, SPIE, 4841, 1739
Ciotti L., Ostriker J. P., Proga D., 2010, ApJ, 717, 708
Cisternas M., et al., 2011, ApJ, 726, 57
Coldwell G. V., Lambas D. G., 2006, MNRAS, 371, 786
Croom S. M., Smith R. J., Boyle B. J., Shanks T., Miller L., Outram P. J., Loaring N. S., 2004, MNRAS, 349, 1397
Croom S. M., et al., 2009, MNRAS, 392, 19
Decarli R., Falomo R., Kotilainen J. K., Hyvönen T., Uslenghi M., Treves A., 2012, AdAst, 2012,
Di Matteo T., Springel V., Hernquist L., 2005, Nature, 433, 604
Djorgovski S., 1991, ASPC, 21, 349
Djorgovski S. G., Odewahn S. C., Gal R. R., Brunner R. J., de Carvalho R. R., 1999, ASPC, 191, 179
Djorgovski S. G., Courbin F., Meylan G., Sluse D., Thompson D., Mahabal A., Glikman E., 2007, ApJ, 662, L1
Dunlop J. S., McLure R. J., Kukula M. J., Baum S. A., O'Dea C. P., Hughes D. H., 2003, MNRAS, 340, 1095
Eftekharzadeh S., Myers A. D., Hennawi J. F., Djorgovski S. G., Richards G. T., Mahabal A. A., Graham M. J., 2017, MNRAS, 468, 77
Falomo R., Treves A., Kotilainen J. K., Scarpa R., Uslenghi M., 2008, ApJ, 673, 694-702

Falomo R., Bettoni D., Karhunen K., Kotilainen J. K., Uslenghi M., 2014, MNRAS, 440, 476
Fanidakis N., Macciò A. V., Baugh C. M., Lacey C. G., Frenk C. S., 2013, MNRAS, 436, 315
Farina E. P., Falomo R., Treves A., 2011, MNRAS, 415, 3163
Farina E. P., Montuori C., Decarli R., Fumagalli M., 2013, MNRAS, 431, 1019
Flesch E. W., 2015, PASA, 32, e010
Foreman G., Volonteri M., Dotti M., 2009, ApJ, 693, 1554
Francis P. J., Drake C. L., Whiting M. T., Drinkwater M. J., Webster R. L., 2001, PASA, 18, 2
Fukugita M., Nakamura O., Schneider D. P., Doi M., Kashikawa N., 2004, ApJ, 603, L65
Green P. J., Myers A. D., Barkhouse W. A., Mulchaey J. S., Bennert V. N., Cox T. J., Aldcroft T. L., 2010, ApJ, 710, 1578
Green P. J., Myers A. D., Barkhouse W. A., Aldcroft T. L., Trichas M., Richards G. T., Ruiz Á., Hopkins P. F., 2011, ApJ, 743, 81
Heckman T. M., Best P. N., 2014, ARA&A, 52, 589
Hennawi J. F., et al., 2006, AJ, 131, 1
Hennawi J. F., et al., 2010, ApJ, 719, 1672
Hennawi J. F., Prochaska J. X., Cantalupo S., Arrigoni-Battaia F., 2015, Sci, 348, 779
Hewett P. C., Wild V., 2010, MNRAS, 405, 2302
Hopkins P. F., Hernquist L., Cox T. J., Kereš D., 2008, ApJS, 175, 356
Jiang N., Wang H., Mo H., Dong X.-B., Wang T., Zhou H., 2016, ApJ, 832, 111
Karhunen K., Kotilainen J. K., Falomo R., Bettoni D., 2014, MNRAS, 441, 1802
Kauffmann G., Haehnelt M., 2000, MNRAS, 311, 576
Kauffmann G., White S. D. M., Heckman T. M., Ménard B., Brinchmann J., Charlot S., Tremonti C., Brinkmann J., 2004, MNRAS, 353, 713
Kayo I., Oguri M., 2012, MNRAS, 424, 1363
Kochanek C. S., Falco E. E., Muñoz J. A., 1999, ApJ, 510, 590
Kocevski D. D., et al., 2012, ApJ, 744, 148
Kormendy J., Ho L. C., 2013, ARA&A, 51, 511
Krolewski A. G., Eisenstein D. J., 2015, ApJ, 803, 4
Kunert-Bajraszewska M., Janiuk A., 2011, ApJ, 736, 125
Liu X., Shen Y., Bian F., Loeb A., Tremaine S., 2014, ApJ, 789, 140
Lynden-Bell D., 1969, Natur, 223, 690
McNamara B. R., Nulsen P. E. J., 2007, ARA&A, 45, 117
Mannucci F., Basile F., Poggianti B. M., Cimatti A., Daddi E., Pozzetti L., Vanzi L., 2001, MNRAS, 326, 745
Mechtley M., et al., 2016, ApJ, 830, 156
Montero-Dorta A. D., Prada F., 2009, MNRAS, 399, 1106
Mortlock D. J., Webster R. L., Francis P. J., 1999, MNRAS, 309, 836
Morselli L., et al., 2014, A&A, 568, A1
Myers A. D., Brunner R. J., Richards G. T., Nichol R. C., Schneider D. P., Bahcall N. A., 2007, ApJ, 658, 99
Myers A. D., Richards G. T., Brunner R. J., Schneider D. P., Strand N. E.,Hall P. B., Blomquist J. A., York D. G., 2008, ApJ, 678, 635
Ostriker J. P., 1980, ComAp, 8, 177
Onoue M., et al., 2017, arXiv, arXiv:1704.06051
Padmanabhan N., White M., Norberg P., Porciani C., 2009, MNRAS, 397, 1862
Pâris I., et al., 2014, A&A, 563, A54
Pâris I., et al., 2017, A&A, 597, A79
Popesso P., Biviano A., 2006, A&A, 460, L23
Porciani C., Magliocchetti M., Norberg P., 2004, MNRAS, 355, 1010
Richards G. T., et al., 2004, ApJS, 155, 257
Richardson J., Zheng Z., Chatterjee S., Nagai D., Shen Y., 2012, ApJ, 755, 30
Salpeter E. E., 1964, ApJ, 140, 796
Sandrinelli A., Falomo R., Treves A., Farina E. P., Uslenghi M., 2014, MNRAS, 444, 1835
Schlegel D. J., Finkbeiner D. P., Davis M., 1998, ApJ, 500, 525
Schneider D. P., et al., 2010, AJ, 139, 2360
Serber W., Bahcall N., Ménard B., Richards G., 2006, ApJ, 643, 68
Sérsic J. L., 1963, BAAA, 6, 41
Shen Y., et al., 2013, ApJ, 778, 98
Shields G. A., Rosario D. J., Junkkarinen V., Chapman S. C., Bonning E. W., Chiba T., 2012, ApJ, 744, 151
Shlosman I., Frank J., Begelman M. C., 1989, Natur, 338, 45
Silverman J. D., et al., 2009, ApJ, 695, 171
Simpson C., Mortlock D., Warren S., Cantalupo S., Hewett P., McLure R., McMahon R., Venemans B., 2014, MNRAS, 442, 3454
Söchting I. K., Clowes R. G., Campusano L. E., 2002, MNRAS, 331, 569
Uslenghi M., Falomo R., 2008, in Modelling and Simula-tion in Science, ed. V. Di Gesu et al. (Hackensack, NJ:World Scientific), p. 313
Villforth C., et al., 2017, MNRAS, 466, 812
Volonteri M., Rees M. J., 2006, ApJ, 650, 669
Zel'dovich Y. B., 1964, SPhD, 9, 195
Zhang S., Wang T., Wang H., Zhou H., 2013, ApJ, 773, 175
Zhdanov V. I., Surdej J., 2001, A&A, 372, 1

APPENDIX A: GTC OPTICAL SPECTRA

In Figures 2 and A1 we show the optical spectra of QSO pairs obtained at GTC. Some notes on individual cases are reported in the following.

J115822.77+123518.5, J115822.98+123520.3 (QP13) - Found by using the kernel density estimation (KDE, Richards et al. 2004), this QSO pair was spectroscopically investigated by Myers et al. (2008) as a close binary QSO candidate. Due to the spectral resolution, component separation and similar colors, Myers et al. (2008) didn't exclude it was a most likely lens candidate. It was, however, recovered as a double QSO by Foreman, Volonteri, & Dotti (2009) and by Green et al. (2011). Dissimilarities in the peak-to-continuum ratios in our GTC spectra, reported in Figure 2, validate the physical nature of the QSO pair.

J124031.42+111848.9, J124032.67+111959.2 (QP14) - Both the spectra are available in the SDSS archives (Schneider et al. 2010; Pâris et al. 2014), but for the B component the [OIII] line positions are not measurable. On the GTC spectrum (Figure A1), a line emerges in the position ascribable to the [O III]λ5007 when compared with the broad MgII line and other minor emissions in the SDSS spectrum. Hβ line appears suppressed in both GTC and SDSS observations.

J125454.86+084652.1, J125455.09+084653.9 (QP 16) - It was spectroscopically identified as close partially resolved binary QSO by Green et al. (2010), who found it hosted in an ongoing galaxy merger with clear tidal tail features. Its environment was investigated by Green et al. (2011) in a multi-wavelength study of binary QSOs, with other QSO pairs of our sample (see Section 1). It was included in our GTC program with the aim to better measure the $\Delta V_{\|}$ through a reliable redshift measure of the B companion. As shown in Figure A1, narrow lines are significantly higher in the A component, while [OIII] lines appear broken off or absent at all, similarly to the spectrum observed by Green et al. (2010) on 2009/05/22. We note that, in comparison, in the spectrum retrieved from the SDSS archives and observed on 2007/06/15, the [O III]λ5007 line appears stronger and the spectral continuum enhanced.

J141855.41+244108.9, J14189+2441B (QP 18) - It was identified as a close QSO pair ($\Delta\theta$=4.5Ó) by Myers et al. (2008), who tended to excluded a single-lensed source due to the low probability associated to pairs with $\Delta\theta$ >3, following Hennawi et al. (2006). However, they did not rule out the lens interpretation for this pair on the basis of their spectroscopy. The pair was included in the QSO binary samples of Foreman, Volonteri, & Dotti (2009), Green et al. (2011) and Eftekharzadeh et al. (2017). Only the spectrum of the

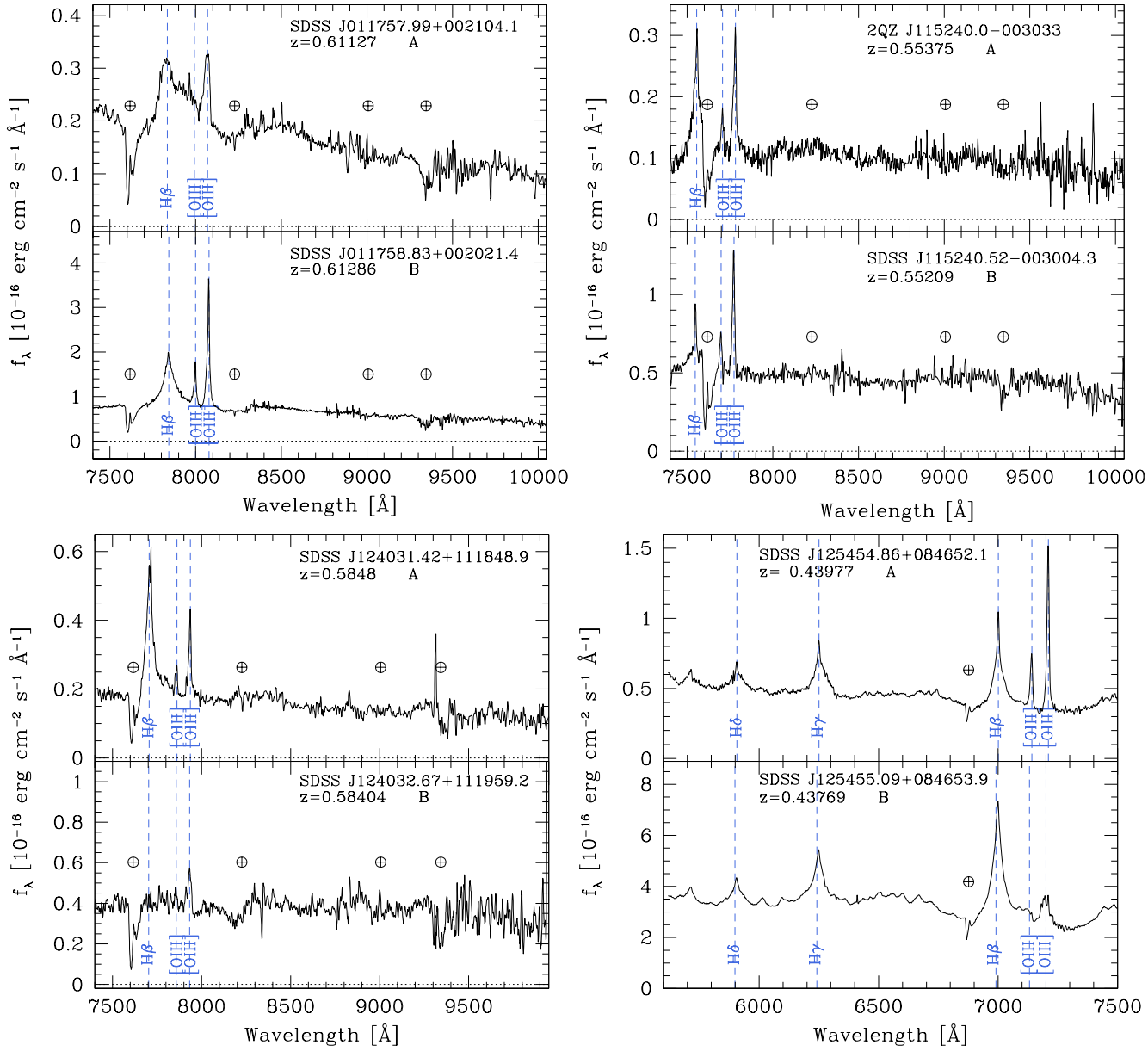

Figure A1. Spectra of the QSO physical pairs observed at GTC. The most prominent emission features are marked. The main telluric bands are indicated by ⊕.

QSO A was recovered in literature (SDSS archives). Due to spectral dissimilarities also in this case we confirm the physical nature the QSO association. In the GTC 2D spectrum we note the presence of a companion galaxy not detected by the SDSS photometry, which is very close to the weaker component of this pairs (QSO B, see Figure A2). It is visible at the [O III]λ5007 and [O III]λ4959 emission line positions at ~ the same redshift of the near QSO, and probably in interaction. Its emissions were carefully separated from the QSO spectrum during the extraction phase.

J164311.34+315618.4, J164311.38+315620.6 (QP 20) - It is one of the closest-known QSO pairs, with projected separation 2.3″corresponding to 15 kpc. Discovered as a binary radio-loud/radio-quiet binary QSO by Brotherton et al. (1999), it contains the only one object detected as radio-loud in our QSO pair sample (FIRST J164311.3+3156184). By using multi-band imaging, Kunert-Bajraszewska & Janiuk (2011) found that the host galaxy of the radio-loud component is highly disturbed. They also observed an intermittent activity of radio structure, possibly due to the rapid change of the jet direction and/or to the interaction with the companion.

APPENDIX B: HOST GALAXIES

Galaxies hosting QSOs were photometrically studied with the aim of outlining their properties and drawing a comparison with those hosting isolated QSOs. The QSO images are drawn in i-band from SDSS-DR12 imaging archives (see Subsection 3.1). We used the

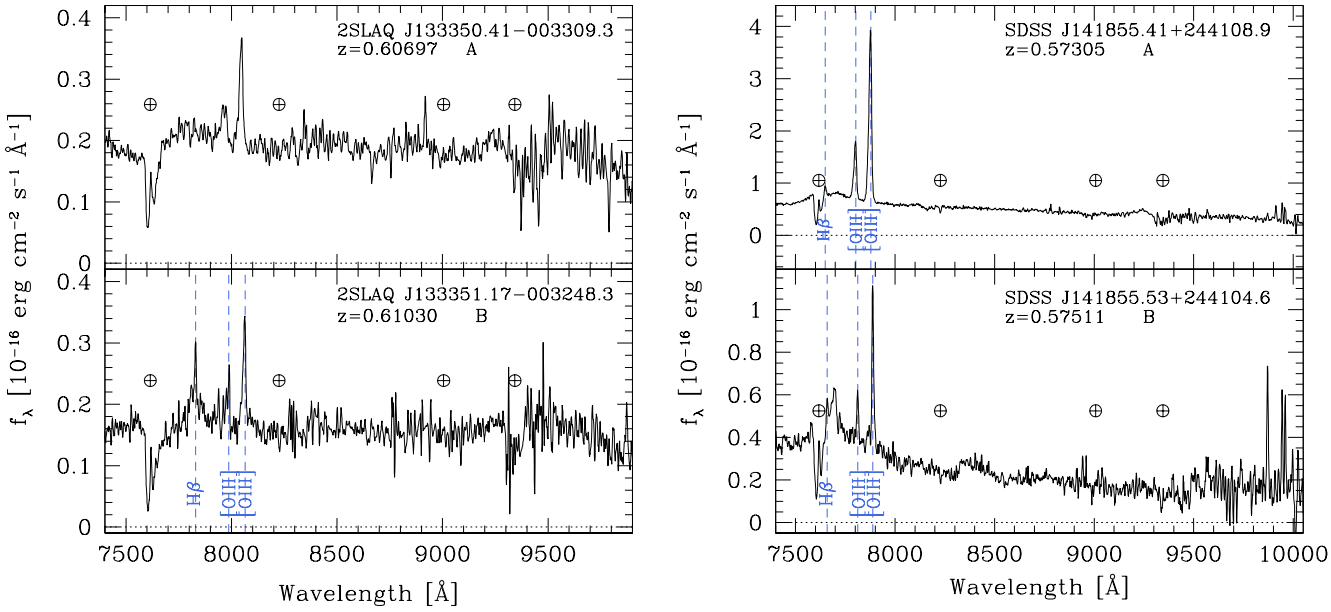

Figure A1. — Continued

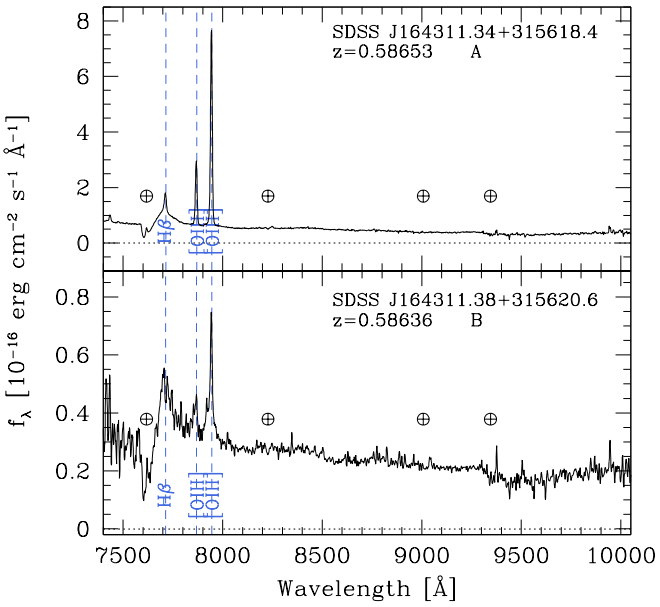

Figure A1. — Continued

Astronomical Image Decomposition and Analysis (AIDA Uslenghi & Falomo 2008) software to model and to decompose the host galaxy luminosity from the nuclear source. The nucleus is described by a local Point Spread Function (PSF) generated through close stars in the image. Host halo may be resolved by a second fit procedure if the luminosity profile results best fitted by the galaxy model represented by a Sérsic (1963) law convolved with the proper PSF. The two fit outputs are compared by the $\chi^2_{PSF}/\chi^2_{PSF+host}$ ratio and visually inspected. Example of fits are given in Figure B1. The employed technique was applied in previous QSO host galaxy studies (e.g. Falomo et al. 2008; Decarli et al. 2012; Sandrinelli et al. 2014) and widely discussed in Falomo et al. (2014).

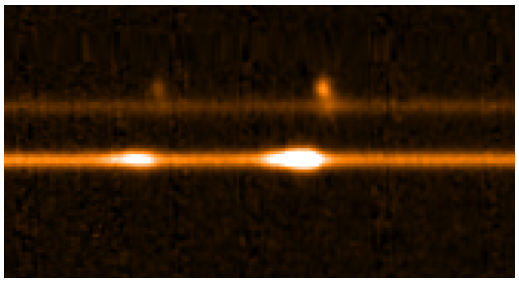

Figure A2. GTC 2D spectra of the QSO pair QP18. The spectrum of QSO A is the brighter one. At ∼ 1.4 arcsec (∼ 9 kpc projected distance) from the spectrum of QSO B, a galaxy is apparent at the [O III]λ5007 and [O III]λ4959 emission line positions at ∼ the same redshift of the near QSO.

The classification results in 18 (45%) resolved host galaxies (R), 8 (20%) marginally resolved (M), and 17 (33%) unresolved (U); for 9 pairs we are able to characterize the host galaxy properties of both QSOs. Nucleus and host galaxy i-magnitudes are reported in Table B1, together with the rest-frame absolute SDSS r-magnitudes, dereddened and k-corrected. Corrections for galactic extinction were taken from SDSS database. K-corrections derive from templates of Mannucci et al. (2001) and Francis et al. (2001) for host galaxies and nuclei, respectively. We find that no obvious differences are apparent in the absolute magnitude distributions of the host galaxies of the two samples. They range between M(r)$_{host}$ =−21 mag and M(r)$_{host}$ =−25.5 mag, with the bulk of galaxies between M* and M*−2. Mean values and medians are similar, respectively (−23.2±0.01) mag and (−23.1±0.01) mag for paired QSOs and (−23.4±0.01) mag and (−23.4±0.01) mag for those that are isolated. The indication is that the two families of QSO are indistinguishable with respect the host luminosity.

This paper has been typeset from a TEX/LATEX file prepared by the author.

Table B1. Properties of nuclei and host galaxies of the QSO pairs.

QSO	Class	i_{nuc} [mag]	i_{host} [mag]	$M_{nuc}(r)$ [mag]	$M(r)_{host}$ [mag]	QSO	Class	i_{nuc} [mag]	i_{host} [mag]	$M_{nuc}(r)$ [mag]	$M(r)_{host}$ [mag]
(a)	(b)	(c)	(d)	(e)	(f)	(a)	(b)	(c)	(d)	(e)	(f)
1A	M	19.90	21.61	-22.71	-21.17	11A	R	20.50	19.98	-22.85	-23.75
1B	R	>22	20.35	>-21	-22.42	11B	R	20.28	21.23	-23.09	-22.51
2A	R	20.21	20.55	-22.98	-22.98	12A	U	20.00	—	-22.93	—
2B	U	18.23	—	-24.96	—	12B	R	19.32	18.84	-23.60	-24.33
3A	R	21.68	19.51	-20.61	-22.86	13A	R	19.63	20.33	-23.50	-23.10
3B	R	20.16	19.03	-22.13	-23.33	13B	M	20.42	20.04	-22.72	-23.39
4A	R	20.72	20.63	-21.92	-22.17	14A	U	19.96	—	-23.22	—
4B	M	18.55	20.09	-24.09	-22.71	14B	R	20.75	19.64	-22.42	-23.81
5A	R	19.19	19.55	-24.26	-24.30	15A	M	19.35	19.34	-22.98	-23.09
5B	M	19.45	19.90	-23.28	-23.00	15B	U	18.30	—	-24.02	—
6A	U	19.94	—	-22.74	—	16A	R	19.76	19.21	-22.69	-23.35
6B	M	20.85	20.44	-22.52	-23.32	16B	U	16.97	—	-25.48	—
7A	R	18.90	19.76	-24.00	-23.35	17A	M	20.22	20.52	-23.05	-23.07
7B	M	18.77	20.43	-24.14	-22.69	17B	R	21.25	20.19	-22.03	-23.43
8A	M	18.83	20.70	-24.09	-22.44	18A	U	18.92	—	-24.11	—
8B	U	18.61	—	-24.30	—	18B	M	20.10	20.80	-22.94	-22.50
9A	R	18.68	19.48	-24.20	-23.63	19A	R	18.29	20.04	-25.13	-23.77
9B	U	19.17	—	-23.72	—	19B	U	20.64	—	-22.79	—
10A	U	19.30	—	-23.76	—	20A	R	19.38	19.06	-23.71	-24.32
10B	U	19.95	—	-23.10	—	20B	R	19.59	19.38	-23.49	-23.99

Notes. (a) Quasar identifier: QSO pair number + QSO component. (b) Resolved (R), marginally resolved (M), unresolved (U) host galaxy. (c) and (d) Apparent i-magnitude of the nucleus and host galaxy. (e) and (f) Absolute r-band magnitude (SDSS system, k-corrected and dereddered) of nucleus and host galaxy.

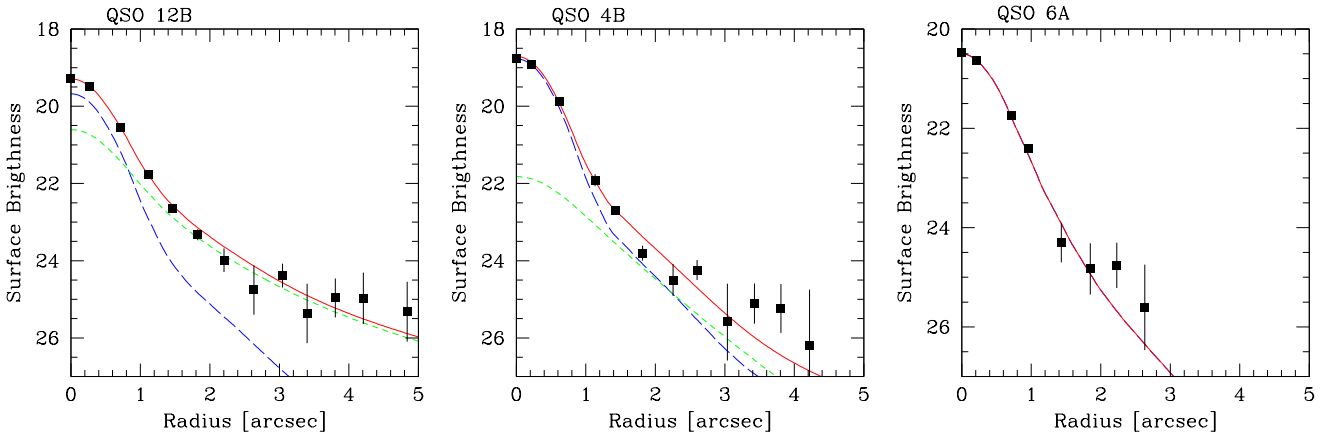

Figure B1. Examples of the QSO luminosity decomposition applied to QSOs with resolved (QSO 12B) marginally resolved (QSO 4B), and unresolved host galaxies (QSO 6A). The average radial brightness profile of the QSO (square dots) is fitted by the scaled point spread function (PSF, green short dashed line) and the host galaxy Sersic law model convolved with the PSF (blue dashed line). The best fit is represented by the solid line